Highly Porous SnO_2 Nanosheet Arrays Sandwiched within TiO_2 and CdS Quantum Dots for Efficient Photoelectrochemical Water Splitting

Zhiwei Wang,[1,+] Xianglin Li,[1,2,+] Chiew Kei Tan,[1] Cheng Qian,[3] Andrew Clive Grimsdale,[1] Alfred Iing Yoong Tok[1,]*

[1]School of Materials Science and Engineering, Nanyang Technological University, Singapore 639798

[2]Hunan First Normal University, No.1015, Fenglin Road (the 3rd), Yuelu District, Changsha, Hunan, China 410205

[3]Division of Physics and Applied Physics, School of Physical and Mathematical Sciences, Nanyang Technological University, Singapore 637371

Email: Prof. Alfred Iing Yoong Tok MIYTok@ntu.edu.sg

[+] These authors contributed equally to this work.

Abstract

A porous SnO_2 nanosheets/TiO_2/CdS quantum dots (SnO_2 NSs/TiO_2/CdS QDs) sandwich structure has been designed and fabricated as a "host-guest" photoanode for efficient solar water splitting applications. In this novel photoanode design, the highly porous SnO_2 NSs serve as the host skeleton for efficient electron collection, while CdS QDs serve as efficient visible light absorbers. A thin interlayer of TiO_2 is introduced for band alignment and reduction of charge recombination. Enhanced photoelectrochemical performance of the as fabricated photoanode is observed with introduction of the TiO_2 interlayer. The optimized host-guest SnO_2 NSs/TiO_2/CdS QDs photoanode shows a photocurrent density as high as 4.7 mA cm^{-2} at 0 V versus

Ag/AgCl, which is 7 times higher than that of the SnO_2 NSs/TiO_2 reference photoanode (0.7 mA cm^{-2}). Furthermore, it also shows lower charge recombination rate compared to the SnO_2 NSs/CdS QDs reference photoanode. Due to the high porosity and transparency of the as developed SnO_2 NSs arrays host, it has great potential in various applications, such as solar energy conversion and energy storage.

Keywords photoanode, host-guest, SnO_2 nanosheet, CdS

1. Introduction

Photoelectrochemical (PEC) water splitting is an effective method to convert unlimited solar energy into clean and storable chemical energy-hydrogen.[1-3] Recently, the host-guest type nanostructured photoelectrodes have attracted much attention due to their high charge collection ability, efficient light absorption and effective charge separation.[4-7] For such structures, the host skeletons generally have high conductivity and large specific surface area, while the photoactive guest materials coated on the host skeleton surface would have high visible light absorption efficiency. Various host-guest photoelectrodes, such as WO_3 nanorod/$BiVO_4$,[8] antimony-doped SnO_2 macropore/Fe_2O_3-nanorod[9] and Al-doped ZnO inverse opals/$BiVO_4$,[10] have been reported for PEC water splitting. A host with high conductivity and specific surface area coupled with an efficient light-absorber guest as well as having good interface band alignment are essential for fabricating efficient host-guest photoelectrodes.[11-15] In PEC water splitting applications, the energy conversion efficiency of the host-guest photoelectrode-based devices are usually undermined by the low electron mobility of the host, inefficient light absorption as well as high charge recombination rate at the interface.[16-19]

Due to its abundance on earth, high stability, high transparency, and potential for

doping with fluorine or antimony, SnO_2 has been considered an ideal host material for photoelectrodes.[20-24] For example, antimony-doped SnO_2 nanorods have reportedly boosted the PEC performance of $BiVO_4$ based photoanode.[25] A fluorine-doped SnO_2/TiO_2 based composite inverse opal structure photoanode has been reported with enhanced PEC performance for solar water splitting applications.[26] Recently, 3D porous SnO_2 nanosheets (NSs) coated on carbon fiber cloth have been reported for lithium battery and electrocatalyst applications due to their high specific surface area.[27, 28] SnO_2 NSs grown on transparent conductive oxide, such as fluorine-doped tin oxide (FTO), can be an ideal host skeleton for host-guest type photoelectrodes because of the high stability, high specific surface area as well as the excellent transparency of SnO_2. CdS quantum dots (QDs) have also been extensively employed as absorber guests in various hybrid photoanodes for PEC applications due to their suitable band structure and efficient visible light absorption.[19, 29-32] The uniform dispersion of CdS QDs on three dimensional SnO_2 host skeletons has been reported for PEC water splitting, such as screw-like SnO_2 nanostructures/CdS QDs.[33] However, the energy conversion efficiency of SnO_2/CdS host-guest photoanodes is greatly limited by the high charge recombination rate at the host/guest interface. TiO_2 has been introduced by researchers to reduce the charge recombination at the SnO_2/CdS host-guest interface.[34, 35]

In this work, we report a 3D SnO_2 NSs/TiO_2/CdS QDs structure as host-guest photoanode for efficient PEC water splitting. Uniform and transparent SnO_2 NSs were grown on the FTO substrate through a hydrothermal reaction followed by a calcination process. Thin TiO_2 interlayer was conformally coated on SnO_2 NSs by atomic layer deposition (ALD), while CdS QDs were assembled on SnO_2 NSs surface by successive ionic layer adsorption and reaction (SILAR) method. The as-prepared

SnO_2 NSs/TiO_2/CdS QDs host-guest photoanode showed better PEC performance than SnO_2 NSs/TiO_2 and SnO_2 NSs/CdS QDs reference photoanodes. The enhanced PEC performance of the SnO_2 NSs/TiO_2/CdS QDs can be attributed to strong visible light absorption from CdS guest, high specific surface area and light trapping effect of the transparent host as well as the good band alignment from the ALD TiO_2 interlayer.

2 Experimental section

2.1 Materials

Tin (IV) chloride pentahydrate ($SnCl_4 \cdot 5H_2O$), thiourea (C_2H_5NS), isopropanol, cadmium nitrate tetrahydrate and sodium sulfide nonahydrate were purchased from Sigma-Aldrich. FTO substrates with a surface resistivity of 8 Ω/sq were procured from Pikington.

2.2 Synthesis of SnO_2 NSs on FTO substrates

FTO substrates (1.5 cm x 5 cm) were sequentially cleaned with acetone, methanol, ethanol and deionized (DI) water and dried with nitrogen flow. The precursor solution was prepared based on existing literatures with $SnCl_4$ (100 mg), C_2H_5NS (100 mg) and isopropanol (25 ml).[27, 28] Then, four pieces of clean FTO substrates were placed standing at opposing walls of a 100 ml Teflon autoclave containing the as-prepared precursor solution. After sealing, the autoclave was transferred to an oven and kept at 200 °C for 24 h. After the hydrothermal reaction, the obtained SnS_2 nanosheet samples were washed with DI water and annealed at 500 °C in an atmospheric environment for 2 h to convert them into SnO_2.

2.3 Coating of SnO_2 NSs with TiO_2 by ALD

A homebuilt ALD system was utilized to deposit a thin film of TiO_2 on the surface of SnO_2 NSs at 80 °C.[36] $TiCl_4$ and water were used as the Ti and oxygen precursors, respectively. A total of 400 ALD cycles were used to deposit ~15 nm TiO_2 conformal layers on the SnO_2 NSs. After ALD of TiO_2, the as-prepared samples were annealed at 500 °C in air for 1 hour for the crystallization of TiO_2.

2.4 Preparation of CdS QDs

The CdS QDs were deposited on the surface of SnO_2 NSs/TiO_2 using the typical SILAR method.[37, 38] Specifically, a SnO_2 NSs/TiO_2 sample was immersed into cadmium nitrate methanol solution for 1 minute and then rinsed with methanol for another minute, followed by drying with nitrogen flow. Next, the sample was immersed into the sodium sulfide solution for 1 minute and rinsed with ethanol solution for another minute, followed by drying with nitrogen flow. The entire procedure was repeated for 15 times. Finally, the sample was annealed at 400 °C for 30 minutes under argon protection.

2.5 Materials Characterization

Field-emission scanning electron microscope (SEM), JEOL, JSM 7600F was used to investigate the microstructure and morphology of the as-prepared samples. X-ray diffraction (XRD) pattern was carried out on a Bruker D8 X-ray diffractometer, equipped with Cu Kα radiation source. UV-Vis diffuse reflectance spectra were collected on a Varian, Cary 5000 spectrum system. Raman spectra were collected on a Renishaw in Via Raman system using 477 and 532 nm as the excitation wavelengths.

2.6 PEC measurements

The PEC performance measurements of the as-prepared samples were carried out on

an Autolab 270 workstation with a three-electrode electrochemical system under AM 1.5G simulated sunlight illumination (100 mW cm^{-2}) from a solar simulator (300W Xe lamp, Newport). The as-prepared photoanodes, Ag/AgCl (3M KCl) and platinum mesh were used as the working electrode, reference electrode and counter electrode, respectively. 0.25 M Na_2SO_3 and 0.35 M Na_2S were used as the electrolyte during the PEC water splitting test. The light intensity of the solar simulator was calibrated to 100 mW cm^{-2} using a standard reference silicon solar cell. The photocatalytic hydrogen generation was measured by a gas chromatograph (Shimadzu GC-2014; Molecular sieve 5A, TCD detector, Ar carrier gas) with 0.25 M Na_2SO_3 and 0.35 M Na_2S as electrolyte under AM 1.5G simulated sunlight illumination. The applied voltage was 0 V versus AgCl and the size of the photoanode is 1.5 cm x 4 cm.

3 Result and discussion

3.1 Fabrication and Characterization of SnO_2 NSs/TiO_2/CdS QDs

The fabrication process of SnO_2 NSs/TiO_2/CdS QDs photoanodes is schematically shown in **Figure 1**. Firstly, SnS_2 nanosheet arrays are grown on the FTO substrates through a hydrothermal reaction. After calcination, the as-grown SnS_2 nanosheet arrays are converted into 3D vertically aligned SnO_2 NSs. Next, conformal TiO_2 films are deposited on the surface of SnO_2 NSs by ALD. Finally, CdS QDs are deposited on the surface of TiO_2 through SILAR method.

For PEC water splitting applications, full coverage of the FTO substrate with photoanode materials is required. Otherwise, the direct contact of the FTO and electrolyte will cause significant dark current and depress the charge separation, hence reducing the entire PEC efficiency. We have found that the amount of chemicals used

144 in the precursor solution played an important role in the coverage of as-grown SnO_2
145 NSs on FTO substrates, as shown in Figures 2(a)-(c). When 40 mg of $SnCl_4$ and 40
146 mg of C_2H_5NS were used for preparing the precursor solution, the SnO_2 NSs coverage
147 of the final product was very poor where a few clusters of SnO_2 NSs were sparsely
148 grown on the FTO surface as shown in Figure 2(a). Figures 2(b&c) show the SEM
149 images of the SnO_2 NSs samples grown with 80 mg of $SnCl_4$ and C_2H_5NS each and
150 100 mg of $SnCl_4$ and C_2H_5NS each, respectively. Figure 2b clearly show that the more
151 clusters of SnO_2 NSs were grown on the FTO substrate with an increased amount of
152 chemicals used in the precursor solution. Full coverage of SnO_2 NSs on FTO were
153 achieved when 100 mg of $SnCl_4$ and C_2H_5NS each were used in the precursor solution,
154 as shown in Figure 2(c). It should be noted that the SnS_2 NSs would partially peel off
155 from FTO substrate after rinsing with DI water when even more $SnCl_4$ and C_2H_5NS
156 were used. Before the thermal conversion of SnS_2 NSs to SnO_2 NSs, SnS_2 NSs were
157 adhere to the FTO, indicating that the mechanism for the increased coverage of SnS_2
158 NSs may involve heterogeneous nucleation and the following growth and
159 aggregation.[39] In the early stage of the hydrothermal reaction, some SnS_2 nuclei
160 were formed on the FTO substrate due to the heterogeneous nucleation. Through the
161 ion-by-ion process, more nuclei would form subsequently, providing sites for the
162 growth of the SnS_2 NSs. When low concentrations of precursors were used, small
163 density of nuclei with large sizes formed on the FTO substrate, thus only few clusters
164 of SnS_2 NSs were obtained. With higher concentrations of precursors, higher density
165 of nuclei of smaller sizes were formed and more SnS_2 NSs were grown on the FTO
166 substrate. Thus, full coverage of SnS_2 NSs, which would be converted to SnO_2 NSs
167 after calcination, on the FTO substrate could be achieved.

168 The as-prepared SnO_2 NSs nanosheets stand vertically on the FTO substrate,

instead of being randomly stacked together, which is beneficial for loading of photoactive guest materials. The vertically growth of SnS_2 NSs can be ascribed to the formation of metal-thiourea complex, which can decrease the amount of free metal ions and sulfur ions, favoring for the oriented growth of SnS_2 NSs.[40] Figure 2(d) shows the magnified SEM view of the as-grown SnO_2 NSs on FTO substrate. A large number of nano-pores could be observed on the SnO_2 nanosheets, indicating high porosity of the as-grown SnO_2 NSs. The high specific surface area of the as-fabricated SnO_2 NSs arrays is also beneficial for loading of more photoactive guest materials and for increasing the contact area of the entire photoanode to electrolytes as well. This enhances the PEC performance of the photoanode.

Due to the self-limiting growth mechanism of ALD, it can be used for deposition of nano-films over 3D nanostructures with excellent conformality. In our study, the as-fabricated SnO_2 NSs were coated with a thin layer of TiO_2 using ALD. In the customized ALD system, N_2 was used as the carried gas while $TiCl_4$ and H_2O were used as precursors. In each cycle of ALD process, $TiCl_4$ reacted with the hydroxyl groups on the surface of SnO_2 NSs and formed Cl_3Ti-O-SnO_2. After the purge of excess $TiCl_4$ and byproduct HCl by N_2, H_2O gas was introduced into the chamber to react with Cl_3Ti-O-SnO_2. Thus, one layer of TiO_2 film was conformally coated on the SnO_2 NSs while excess H_2O and the byproduct HCl gas were purged by N_2. The thickness of TiO_2 films can be controlled by varying the number of ALD cycles. From Figures 2(e), it could be clearly seen that the sheet-like structure remains unchanged, indicating the conformal coating of TiO_2 films over SnO_2 NSs. The average thickness of the SnO_2 NSs increases from a few nanometers to around 30 nm after 400 cycles of ALD TiO_2 films. The uniform coating of TiO_2 films over SnO_2 NSs could also be observed from the smooth surface. After loading of CdS QDs, the smooth surface

becomes coarse and the thickness of the nanosheet further increases to around 40 nm, as shown in Figure 2(f). During the SILAR process, Cd^{2+} ions were first adsorbed onto the TiO_2 surface and then reacted with S^{2-} ions to form CdS particles. Energy-dispersive X-ray spectroscopy study further confirmed the existence of Cd, S, Ti, O and Sn elements in the SnO_2 NSs/TiO_2/CdS QDs photoanode, as shown in Figure S1.

XRD was utilized to determine the crystallinity and constituent of the as-prepared samples. Figure 3(a) shows the XRD patterns of bare FTO substrate, SnO_2 NSs, SnO_2 NSs/TiO_2 and SnO_2 NSs/TiO_2/CdS QDs. The diffraction peaks of SnO_2 NSs at 27°, 34°, 38°, 52° and 55° correspond to (110), (101), (200), (211) and (220) planes of the rutile structure of SnO_2. As both SnO_2 NSs and FTO are comprised of rutile SnO_2, the XRD peaks of SnO_2 NSs and FTO overlap. However, the XRD peaks can be distinguished by their different full width at half maximum (FWHM). The FWHM of the XRD peaks for SnO_2 NSs are much broader than that for FTO substrate, indicating that SnO_2 NSs are composed by nanosized SnO_2 crystals, which is consistent with our SEM study, as shown in Figure 2(d). After coating of ALD TiO_2, small but obvious diffraction peaks located at 28°, 36° and 41° could be observed, which can be ascribed to the (110), (101) and (200) planes of rutile phase TiO_2. Through the comparison of the XRD patterns of SnO_2 NSs/TiO_2 and SnO_2 NSs /TiO_2/CdS QDs, two new obvious diffraction peaks located at 29° and 44° could be observed after deposition of CdS QDs, and they can be ascribed to the (101) and (110) planes of hexagonal phase CdS. Raman spectroscopy was further utilized to determine the compositions and crystal structures of the as-prepared hybrid nanostructures. Figure 3(b) shows the Raman spectra of FTO substrate and SnO_2 NSs. Due to the high transparency of SnO_2 NSs, the incident light is able to penetrate through the SnO_2

NSs array and reach the FTO substrate, which causes unavoidably strong background signals of FTO substrate. The pure FTO substrate has one obvious peak located at 557 cm^{-1}, which is consistent with previous reports.[41] After growth of SnO_2 NSs, another weak but obvious peak located at 632 cm^{-1} could be observed, which can be ascribed to A_{1g} mode of SnO_2. As compared to XRD, Raman could clearly indicate the successful fabrication of SnO_2 NSs on FTO substrate. Figure 3(c) presents the Raman spectra of SnO_2 NSs/TiO_2 and SnO_2 NSs/TiO_2/CdS QDs. For the spectrum of SnO_2 NSs/TiO_2 (red curve in Figure 3c), the peaks located at 236 cm^{-1} (broad band), 443 cm^{-1} (Eg) and 610 cm^{-1} (A1g) can be ascribed to rutile phase of TiO_2,[41] which is consistent with our XRD study. The new peak located at 304 cm^{-1} observed in the Raman spectrum of SnO_2 NSs/TiO_2/CdS QDs corresponds to the 1LO optical phonons of CdS.[35] Thus, both Raman peaks of TiO_2 and CdS can be observed. The disappearance of Raman peaks of SnO_2 at 632 cm^{-1} might be caused by the limited penetration depth of laser used in the Raman testing or the relative weak signals of SnO_2. The step by step Raman testing as well as XRD characterization indicate the successful fabrication of the composite SnO_2 NSs/TiO_2/CdS QDs.

Figure 3(d) shows the UV-Vis absorption spectra of SnO_2 NSs/TiO_2 and SnO_2 NSs/TiO_2/CdS QDs. The SnO_2 NSs/TiO_2 sample has light absorption merely in the UV range due to the wide bandgaps of SnO_2 (3.6 eV) and TiO_2 (3.2 eV). However, the light absorption spectrum edge of SnO_2 NSs/TiO_2 extends to the visible area of up to around 550 nm. This is due to the introduction of CdS QDs which have a smaller bandgap of 2.4 eV. Since visible light accounts for a large part of solar energy, photoanodes with strong visible light absorption should have higher PEC performance for water splitting application.

3.2 PEC performance of SnO_2 NSs/TiO_2/CdS QDs photoanode

The PEC performance of the as-prepared samples was evaluated by linear sweep voltammetry with a three-electrodes system. The as-prepared samples, platinum sheet, Ag/AgCl were used as the photoanode, cathode and reference electrode respectively. A 0.25 M Na_2S and 0.35 M Na_2SO_3 aqueous solution was used as the electrolyte. As counter electrode platinum sheet has little effect on the generated photocurrent, the photocurrent density-potential characteristics can be used to determine the performance and nature of the photoanode. With higher photocurrent, larger amount of photogenerated electrons can be involved in the hydrogen evolution on the counter electrode platinum sheet.[42] Figure 4(a) shows the comparison of linear sweep curves of the SnO_2 NSs/TiO_2, SnO_2 NSs/CdS-QDs, and SnO_2 NSs/TiO_2/CdS QDs photoanodes collected under both dark and illumination conditions. It can be clearly observed that the SnO_2 NSs/TiO_2/CdS QDs photoanodes show much better PEC performance than the SnO_2 NSs/TiO_2 and SnO_2 NSs/CdS QDs photoanodes. The photocurrent density of the SnO_2 NSs /TiO_2/CdS QDs photoanode reaches 4.7 mA cm^{-2} at 0 V versus AgCl, which is almost 7 times higher than that of the SnO_2 NSs/TiO_2 photoanode (0.7 mA cm^{-2}). The reason behind this is due to the introduction of CdS QDs which increases the light absorption in the visible range. This is consistent with our UV-Vis study, as shown in Figure 3(d). Besides the increase in photocurrent density, the onset potential of SnO_2 NSs/TiO_2/CdS-QDs photoanode has also dropped from -0.75 V for SnO_2 NSs/TiO_2 photoanode to -1 V and that could also be due to the introduction of CdS QDs in the photoanode. To further determine the role of TiO_2 interlayer, the linear sweep curve of SnO_2 NSs/CdS QDs photoanode was also collected, as seen in the black curve in Figure 4(a). It could be clearly seen that the photocurrent density of SnO_2 NSs/CdS QDs photoanode is much smaller than that of the SnO_2 NSs/TiO_2/CdS QDs photoanode with the applied voltage near the onset

potential of SnO_2 NSs/CdS QDs photoanode at around -0.8 V versus Ag/AgCl. This could be due to the charge recombination rate of SnO_2 NSs/CdS QDs photoanode being much higher than that of the photoanode with TiO_2 interlayer.[43] With increased applied voltage, the photocurrent difference between the SnO_2 NSs/CdS QDs and SnO_2 NSs/TiO_2/CdS QDs photoanodes becomes smaller, which is understandable as the increased applied voltage can depress the charge recombination process. Figure 4(b) shows the linear sweep curves of the SnO_2 NSs/TiO_2, SnO_2 NSs/CdS QDs and SnO_2 NSs/TiO_2/CdS QDs electrodes under chopped light illumination, which agrees well with the difference between their photocurrent and dark current showed in Figure 4(a).

The measurement of actual hydrogen evolution of SnO_2 NSs/TiO_2/CdS QDs was performed at 0 V versus Ag/AgCl in a 0.25 M Na_2S and 0.35 M Na_2SO_3 mixture electrolyte solution. The amount of produced hydrogen gas in the sealed PEC cell was determined by a gas chromatograph. As shown in Fig. S2, the overall hydrogen generated increases with the illumination time with almost constant hydrogen generation rate, indicating the high stability of the as-prepared photoanode. The hydrogen generation rate of SnO_2 NSs/TiO_2/CdS QDs is 7.6 μmol mA^{-1} h^{-1}, which is comparable to hydrogen generation rate reported for another CdS-based photoanode in the literature.[44]

The band alignment and charge transfer process of SnO_2 NSs/TiO_2/CdS QDs photoanode are schematically shown in Figure 5(a). The band edge position of SnO_2, TiO_2 and CdS are favorable for charge transfer.[34, 35] Under light illumination, photo-generated electrons of CdS are sequentially transported from its conductive band (CB) level to lower CB of TiO_2 and then to even lower CB of SnO_2. These photogenerated electrons would then to the conductive FTO substrate and finally to

294 the counter Pt electrode for hydrogen evolution. The holes transfer conversely from
295 valence band (VB) of SnO_2 to higher VB of TiO_2 and even higher VB of CdS for
296 oxidation of S_2^{2-} to $2S^{2-}$. The enhancement in the photocurrent of SnO_2 NSs/TiO_2/CdS
297 QDs photoanode compared to that of SnO_2 NSs/TiO_2 can be ascribed to the visible
298 light absorption of CdS QDs with a band gap of 2.4 eV, while TiO_2 (3.2 eV) and SnO_2
299 (3.6 eV) can only absorb UV light. As visible light accounts for a larger part in the
300 sunlight as compared to UV light, with the same light illumination, more absorption
301 of visible light means there will be more photogenerated electron-hole pairs in the
302 photoanode. In addition, the good band alignment between CdS QDs, TiO_2 and SnO_2
303 provides fast and direct electron pathways, hence enhancing charge separation and
304 reducing the charge recombination rate. Furthermore, the vertically aligned sheet-like
305 and porous structures provide high specific surface area for loading of CdS QDs
306 without stacking. Transparent SnO_2 NSs also ensure effective light transmission
307 inside the hybrid nanostructures, as schematically shown in Figure 5(b). The light
308 illuminated on one side of a single hybrid nanosheet can penetrate through the
309 transparent SnO_2 NSs and reach the CdS and TiO_2, and even the adjacent dwarf
310 nanosheets, on the other side. This means that the incident light can be absorbed for
311 multiple times by CdS QDs.

312 The photocurrent of some SnO_2/CdS based hybrid photoanodes collected at 0.9 V
313 versus RHE with AM 1.5 illumination (100 mW cm^{-2}) is summarized in the Table 1. It
314 can be seen that the nanostructure and composition have a great impact on the PEC
315 performance. Although the photocurrent of the as-prepared SnO_2 NSs/TiO_2/CdS QDs
316 is not the highest, the improved PEC performance due to the introduction of TiO_2
317 layer points out a possible solution to enhance PEC performance of CdS and other
318 existing semiconductors. The PEC performance of the SnO_2 NSs/TiO_2/CdS QDs

photoanode could be further improved by increasing the conductivity of SnO_2 NSs host via doping with antimony or fluorine, which will be part of our future work.

4. Conclusion

In summary, a SnO_2 NSs/TiO_2/CdS QDs host-guest type photoanode has been designed and fabricated for solar water splitting application through a combination of hydrothermal method, ALD technique and typical SILAR method. The density of the as-grown SnO_2 NSs can be tuned by the amount of chemicals used in the precursor solution for the hydrothermal reaction. To reduce the charge recombination rate between CdS guest and SnO_2 host, a thin TiO_2 interlayer has been introduced for band alignment of the host-guest photoanode. The optimized SnO_2 NSs/TiO_2/CdS QDs guest-host photoanode shows better PEC performance compared to SnO_2 NSs/CdS QDs and SnO_2 NSs/TiO_2 reference photoanodes. This enhanced PEC performance is attributed to the high visible light absorption of the CdS guest, large specific surface area and effective light trapping effect from the SnO_2 NSs host as well as the good band alignment from the ALD TiO_2 interlayer. Due to the high porosity and transparency of the as-developed SnO_2 NSs array host, it has great potential in applications in various fields, such as photoelectrodes for solar hydrogen generation, energy storage and smart windows.

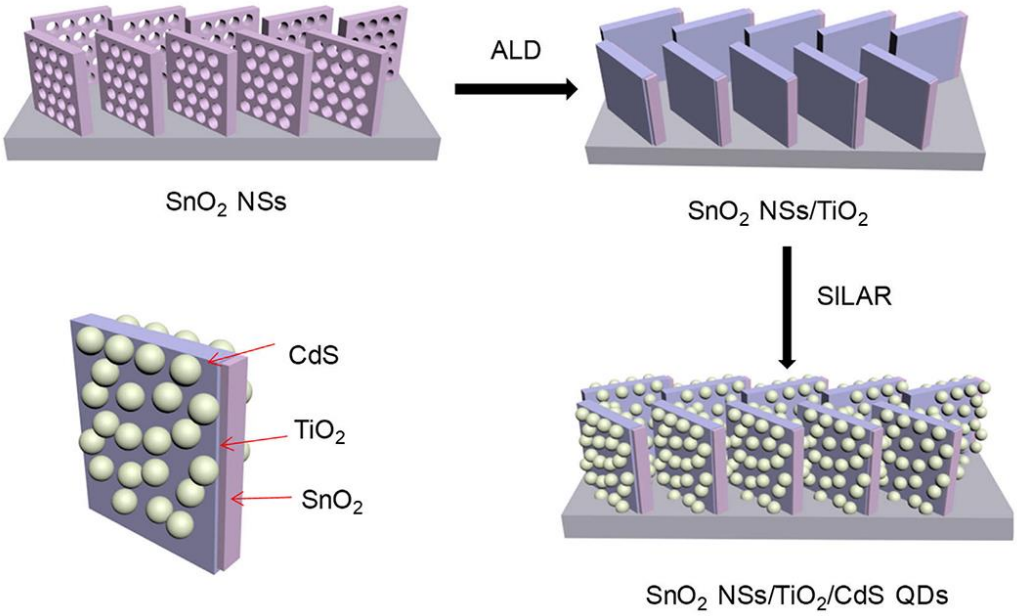

339

340 **Figure 1** Schematic illustration for the fabrication process of the SnO_2 NSs/TiO_2/CdS

341 QDs.

342

343

344

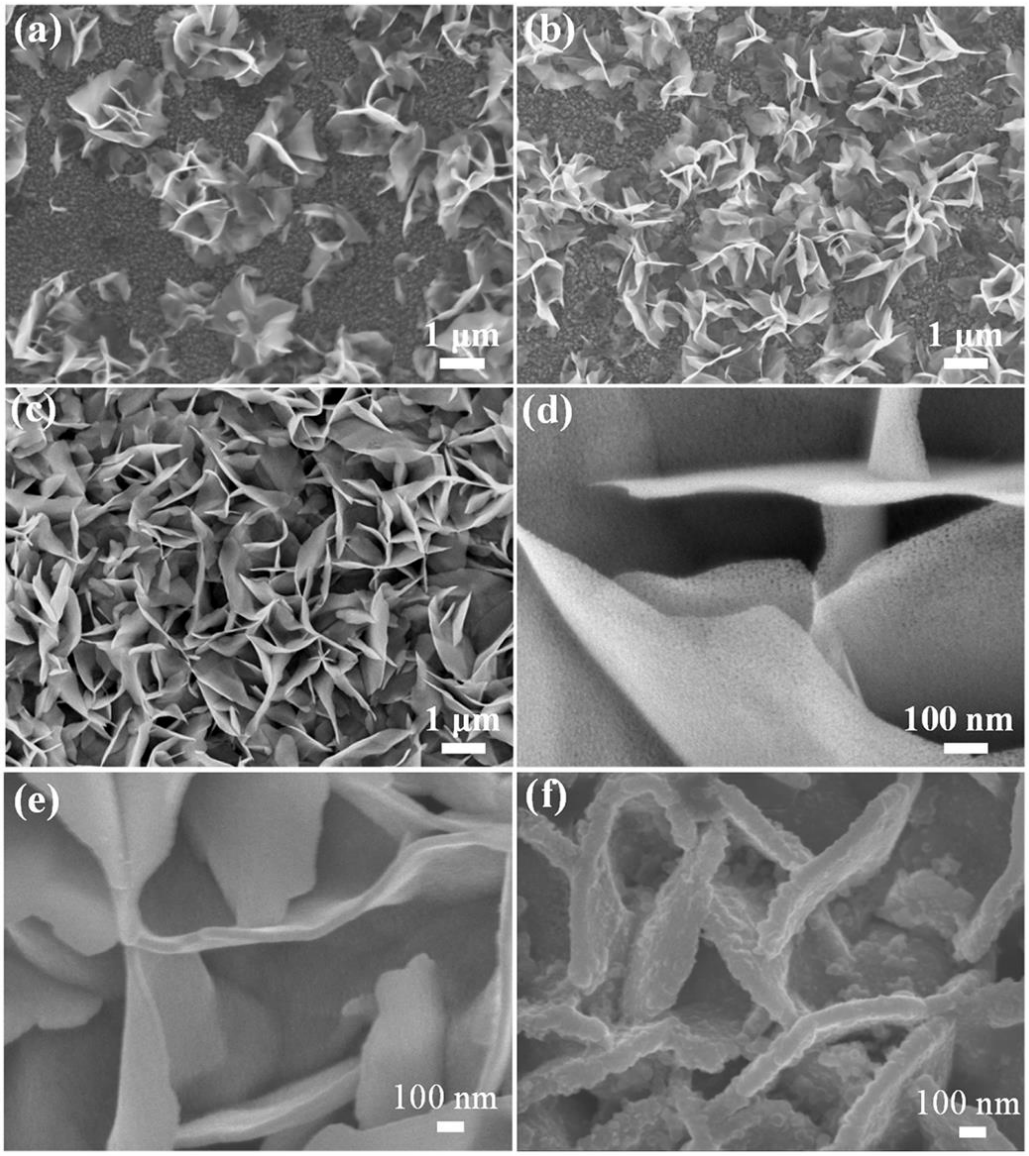

Figure 2 SEM images of: (a) SnO_2 NSs prepared with $SnCl_4$ (40 mg) and C_2H_5NS (40 mg), (b) SnO_2 NSs prepared with $SnCl_4$ (80 mg) and C_2H_5NS (80 mg), (c) SnO_2 NSs prepared with $SnCl_4$ (100 mg) and C_2H_5NS (100 mg), (d) SnO_2 NSs with high magnification. (e) SnO_2 NSs/TiO_2, (f) SnO_2 NSs/TiO_2/CdS QDs.

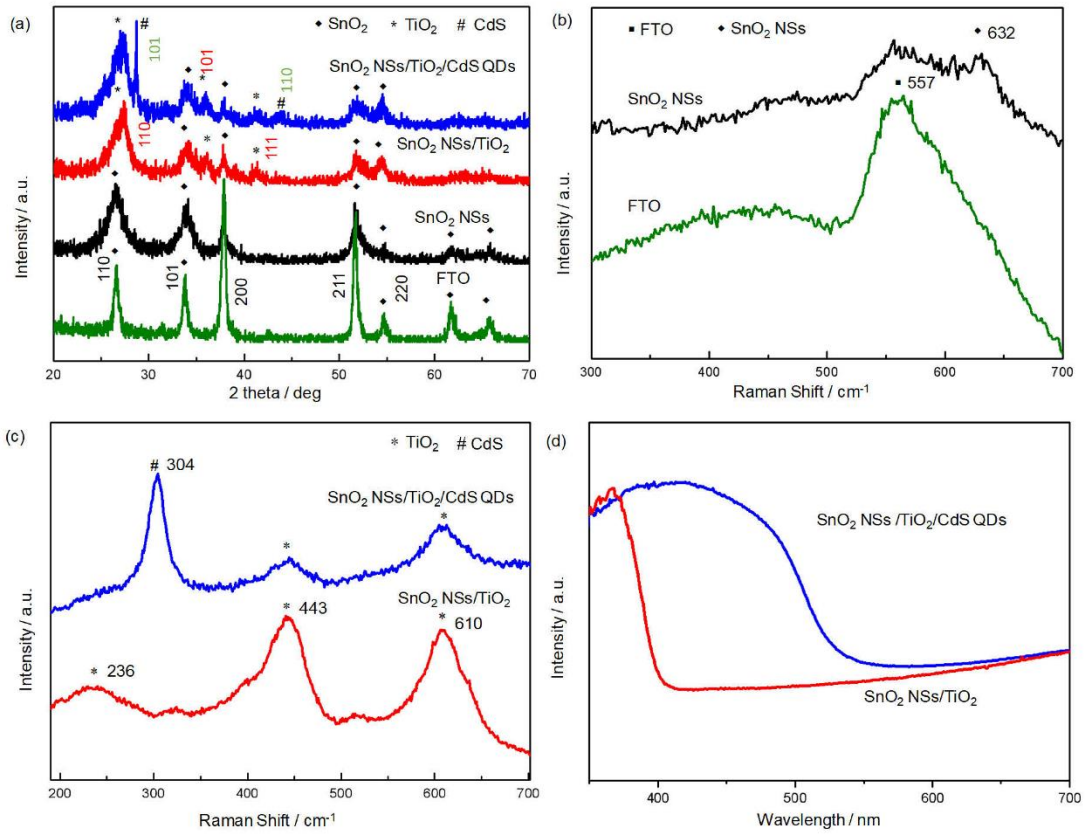

350

351 **Figure 3** (a) XRD patterns of FTO substrate, SnO_2 NSs, SnO_2 NSs/TiO_2 and SnO_2

352 NSs/TiO_2/CdS QDs. (b) Raman spectra of FTO substrate, SnO_2 NSs. (c) Raman

353 spectra of SnO_2 NSs/TiO_2 and SnO_2 NSs/TiO_2/CdS QDs. (d) UV-Vis absorbance of

354 SnO_2 NSs/TiO_2 and SnO_2 NSs/TiO_2/CdS QDs.

355

356

357

358

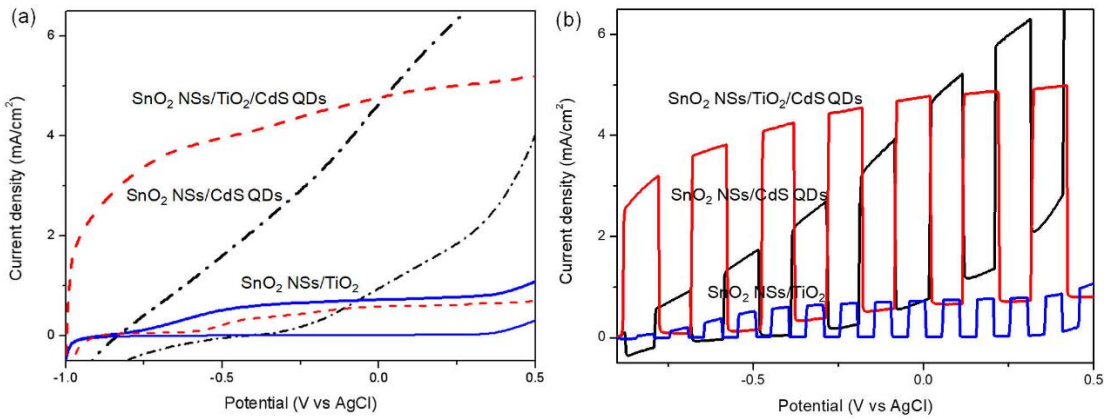

Figure 4 (a) Linear sweep voltammetry measurement of SnO_2 NSs/TiO_2, SnO_2 NSs/CdS QDs and SnO_2 NSs/TiO_2/CdS QDs. (b) Linear sweep voltammetry measurement of SnO_2 NSs/TiO_2, SnO_2 NSs/CdS QDs and SnO_2 NSs/TiO_2/CdS QDs under chopped light illumination.

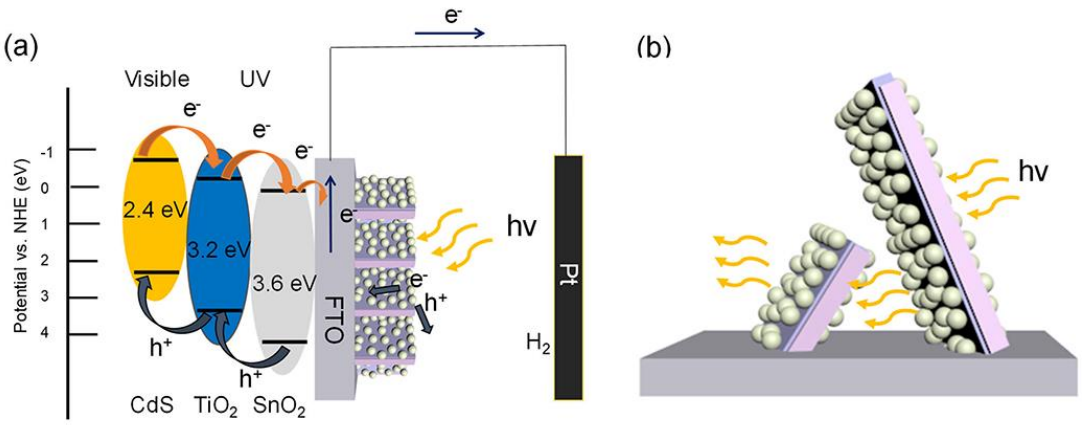

Figure 5 (a) Scheme of band alignment and charge transfer process in the SnO_2 NSs/TiO_2/CdS QDs photoanode. The bandgap of CdS, TiO_2 and SnO_2 are 2.4 eV, 3.2 eV and 3.6 eV, respectively. (b) Scheme of light transmission inside the hybrid SnO_2 NSs/TiO_2/CdS QDs photoanode.

372

373 **Table 1** Comparison of PEC performance of reported SnO_2/CdS based nanostructured
374 photoanodes.

SnO_2/CdS based photoanodes	Electrolyte	Photocurrent density [mA cm^{-2}][a)]	Remarks
SnO_2 NSs/TiO_2/CdS QD	a mixture of 0.25 M Na_2S and 0.35 M Na_2SO_3 aqueous solution	4.7	This work
SnO_2 nanorods/CdS films		1.38	[45]
SnO_2/TiO_2 sea urchinlike nanotube arrays/CdS QDs		2.8	[34]
SnO_2 nanobowl arrays/CdS-NRs		3.5	[46]
SnO_2 nanowires/TiO_2 nanoneedles/CdS QDs		9	[35]
Screw-like SnO_2 nanostructures/CdS QDs		10	[33]

375 [a)]The photocurrent density was collected at 0.9 V vs. reversible hydrogen electrode under AM 1.5
376 illumination (100 mW cm^{-2}).

377

378

379 ## Conflicts of interest

380 There are no conflicts of interest to declare.

381

382 ## Acknowledgments

383 The authors would like to acknowledge funding support from the Singapore Ministry
384 of Education Tier 2 Academic Research Fund (MOE2014-T2-2-082) for this project.

The authors would like to thank Dr. Zhao Xin for his help on the measurement of hydrogen evolution.

References

[1] X. Zhang, B. Zhang, Y. Luo, X. Lv, Y. Shen, Phosphate modified N/Si co-doped rutile TiO_2 nanorods for photoelectrochemical water oxidation, Appl. Surf. Sci. 391 (2017) 288-294.

[2] C. Jiang, S.J. Moniz, A. Wang, T. Zhang, J. Tang, Photoelectrochemical devices for solar water splitting-materials and challenges, Chem. Soc. Rev. 46 (2017) 4645-4660.

[3] X. Li, P.S. Bassi, P.P. Boix, Y. Fang, L.H. Wong, Revealing the role of TiO_2 surface treatment of hematite nanorods photoanodes for solar water splitting, ACS Appl. Mater. Interface 7 (2015) 16960-16966.

[4] X. Li, J. Yu, J. Low, Y. Fang, J. Xiao, X. Chen, Engineering heterogeneous semiconductors for solar water splitting, J. Mater. Chem. A 3 (2015) 2485-2534.

[5] S.J. Moniz, S.A. Shevlin, D.J. Martin, Z.-X. Guo, J. Tang, Visible-light driven heterojunction photocatalysts for water splitting-a critical review, Energy Environ. Sci. 8 (2015) 731-759.

[6] C. Ding, J. Shi, Z. Wang, C. Li, Photoelectrocatalytic water splitting: significance of cocatalysts, electrolyte, and interfaces, ACS Catal. 7 (2016) 675-688.

[7] Y. Zhou, L. Zhang, L. Lin, B.R. Wygant, Y. Liu, Y. Zhu, Y. Zheng, C.B. Mullins, Y. Zhao, X. Zhang, Highly efficient photoelectrochemical water splitting from hierarchical $WO_3/BiVO_4$ nanoporous sphere arrays, Nano Lett. 17 (2017) 8012-8017.

[8] P.M. Rao, L. Cai, C. Liu, I.S. Cho, C.H. Lee, J.M. Weisse, P. Yang, X. Zheng, Simultaneously efficient light absorption and charge separation in $WO_3/BiVO_4$ core/shell nanowire photoanode for photoelectrochemical water oxidation, Nano Lett.

410 14 (2014) 1099-1105.
411 [9] Y.F. Xu, H.S. Rao, B.X. Chen, Y. Lin, H.Y. Chen, D.B. Kuang, C.Y. Su, Achieving
412 highly efficient photoelectrochemical water oxidation with a $TiCl_4$ treated 3D
413 antimony-doped SnO_2 macropore/branched α-Fe_2O_3 nanorod heterojunction
414 photoanode, Adv. Sci. 2 (2015) 1500049.
415 [10] L. Zhang, E. Reisner, J.J. Baumberg, Al-doped ZnO inverse opal networks as
416 efficient electron collectors in $BiVO_4$ photoanodes for solar water oxidation, Energy
417 Environ. Sci. 7 (2014) 1402-1408.
418 [11] X.D. Wang, Y.F. Xu, B.X. Chen, N. Zhou, H.Y. Chen, D.B. Kuang, C.Y. Su, 3D
419 cathodes of cupric oxide nanosheets coated onto macroporous antimony-doped tin
420 oxide for photoelectrochemical water splitting, ChemSusChem 9 (2016) 3012-3018.
421 [12] M.S. Prévot, Y. Li, N. Guijarro, K. Sivula, Improving charge collection with
422 delafossite photocathodes: a host-guest $CuAlO_2$/$CuFeO_2$ approach, J. Mater. Chem. A
423 4 (2016) 3018-3026.
424 [13] S. Cao, X. Yan, Z. Kang, Q. Liang, X. Liao, Y. Zhang, Band alignment
425 engineering for improved performance and stability of $ZnFe_2O_4$ modified CdS/ZnO
426 nanostructured photoanode for PEC water splitting, Nano Energy 24 (2016) 25-31.
427 [14] Z. Zhang, Y. Li, X. Jiang, W. Han, M. Xie, F. Wang, E. Xie, Significantly
428 improved charge collection and interface injection in 3D $BiVO_4$ based multilayered
429 core-shell nanowire photocatalysts, Nanoscale 9 (2017) 14015-14022.
430 [15] S.-Y. Chen, J.-S. Yang, J.-J. Wu, Three-dimensional undoped crystalline SnO_2
431 nanodendrite arrays enable efficient charge separation in $BiVO_4$/SnO_2 heterojunction
432 photoanodes forphotoelectrochemical water splitting, ACS Appl. Energy Mater. 1
433 (2018) 2143-2149.
434 [16] S.K. Karuturi, J. Luo, C. Cheng, L. Liu, L.T. Su, A.I.Y. Tok, H.J. Fan, A novel

435 photoanode with three-dimensionally, hierarchically ordered nanobushes for highly
436 efficient photoelectrochemical cells, Adv. Mater. 24 (2012) 4157-4162.
437 [17] I. Kondofersky, H.K. Dunn, A. Müller, B. Mandlmeier, J.M. Feckl, D.
438 Fattakhova-Rohlfing, C. Scheu, L.M. Peter, T. Bein, Electron collection in host-guest
439 nanostructured hematite photoanodes for water splitting: the influence of scaffold
440 doping density, ACS Appl. Mater. Interface 7 (2015) 4623-4630.
441 [18] Y. Li, X. Wei, B. Zhu, H. Wang, Y. Tang, T.C. Sum, X. Chen, Hierarchically
442 branched Fe_2O_3@TiO_2 nanorod arrays for photoelectrochemical water splitting: facile
443 synthesis and enhanced photoelectrochemical performance, Nanoscale 8 (2016)
444 11284-11290.
445 [19] R.-B. Wei, P.-Y. Kuang, H. Cheng, Y.-B. Chen, J.-Y. Long, M.-Y. Zhang, Z.-Q.
446 Liu, Plasmon-enhanced photoelectrochemical water splitting on gold nanoparticle
447 decorated ZnO/CdS nanotube arrays, ACS Sustain. Chem. Eng. 5 (2017) 4249-4257.
448 [20] G. Yun, M. Balamurugan, H.-S. Kim, K.-S. Ahn, S.H. Kang, Role of WO_3 layers
449 electrodeposited on SnO_2 inverse opal skeletons in photoelectrochemical water
450 splitting, J. Phys. Chem. C 120 (2016) 5906-5915.
451 [21] Y. Gun, G.Y. Song, V.H.V. Quy, J. Heo, H. Lee, K.-S. Ahn, S.H. Kang, Joint
452 effects of photoactive TiO_2 and fluoride-doping on SnO_2 inverse opal
453 nanoarchitecture for solar water splitting, ACS Appl. Mater. Interface 7 (2015)
454 20292-20303.
455 [22] I.A. Cordova, Q. Peng, I.L. Ferrall, A.J. Rieth, P.G. Hoertz, J.T. Glass, Enhanced
456 photoelectrochemical water oxidation via atomic layer deposition of TiO_2 on
457 fluorine-doped tin oxide nanoparticle films, Nanoscale 7 (2015) 8584-8592.
458 [23] L. Wang, A. Palacios-Padrós, R. Kirchgeorg, A. Tighineanu, P. Schmuki,
459 Enhanced photoelectrochemical water splitting efficiency of a hematite-ordered Sb:

460 SnO_2 host-guest system, ChemSusChem 7 (2014) 421-424.
461 [24] S. Zhou, R. Tang, L. Zhang, L. Yin, Au nanoparticles coupled three-dimensional
462 macroporous $BiVO_4/SnO_2$ inverse opal heterostructure for efficient
463 photoelectrochemical water splitting, Electrochim. Acta 248 (2017) 593-602.
464 [25] L. Zhou, C. Zhao, B. Giri, P. Allen, X. Xu, H. Joshi, Y. Fan, L.V. Titova, P.M.
465 Rao, High light absorption and charge separation efficiency at low applied voltage
466 from Sb-doped $SnO_2/BiVO_4$ core/shell nanorod-array photoanodes, Nano Lett. 16
467 (2016) 3463-3474.
468 [26] Z. Wang, X. Li, H. Ling, C.K. Tan, L.P. Yeo, A.C. Grimsdale, A.I.Y. Tok, 3D
469 FTO/FTO-nanocrystal/TiO_2 composite inverse opal photoanode for efficient
470 photoelectrochemical water splitting, Small 14 (2018) 1800395.
471 [27] F. Li, L. Chen, G.P. Knowles, D.R. MacFarlane, J. Zhang, Hierarchical
472 mesoporous SnO_2 nanosheets on carbon cloth: a robust and flexible electrocatalyst for
473 CO_2 reduction with high efficiency and selectivity, Angew. Chem. Int. Edit. 56 (2017)
474 505-509.
475 [28] M. Wang, L. Fan, X. Wu, D. Tian, J. Cheng, Y. Qiu, H. Wu, B. Guan, N. Zhang,
476 K. Sun, Hierarchical mesoporous SnO_2 nanosheets on carbon cloth toward enhancing
477 the polysulfides redox for lithium-sulfur batteries, J. Mater. Chem. A 5 (2017)
478 19613-19618.
479 [29] F. Zhan, W. Liu, H. Li, Y. Yang, M. Wang, Ce-doped CdS quantum dots
480 sensitized TiO_2 nanorod films with enhanced visible-light photoelectrochemical
481 properties, Appl. Surf. Sci. 45 (2018) 476-483.
482 [30] S.K. Karuturi, R. Yew, P.R. Narangari, J. Wong-Leung, L. Li, K. Vora, H.H. Tan,
483 C. Jagadish, CdS/TiO_2 photoanodes via solution ion transfer method for highly
484 efficient solar hydrogen generation, Nano Futures 2 (2018) 015004.

485 [31] Y. Liu, Z. Kang, H. Si, P. Li, S. Cao, S. Liu, Y. Li, S. Zhang, Z. Zhang, Q. Liao,
486 Cactus-like hierarchical nanorod-nanosheet mixed dimensional photoanode for
487 efficient and stable water splitting, Nano Energy 35 (2017) 189-198.
488 [32] S. Ren, Y. Wang, G. Fan, R. Gao, W. Liu, Sandwiched ZnO@ Au@ CdS nanorod
489 arrays with enhanced visible-light-driven photocatalytical performance,
490 Nanotechnology 28 (2017) 465403.
491 [33] Z. Zhang, C. Gao, Z. Wu, W. Han, Y. Wang, W. Fu, X. Li, E. Xie, Toward
492 efficient photoelectrochemical water-splitting by using screw-like SnO_2
493 nanostructures as photoanode after being decorated with CdS quantum dots, Nano
494 Energy 19 (2016) 318-327.
495 [34] C. Li, H. Zhang, C. Cheng, CdS/CdSe co-sensitized 3D SnO_2/TiO_2 sea
496 urchin-like nanotube arrays as an efficient photoanode for photoelectrochemical
497 hydrogen generation, RSC Adv. 6 (2016) 37407-37411.
498 [35] C. Gao, Z. Zhang, X. Li, L. Chen, Y. Wang, Y. He, F. Teng, J. Zhou, W. Han, E.
499 Xie, Synergistic effects in three-dimensional SnO_2/TiO_2/CdS multi-heterojunction
500 structure for highly efficient photoelectrochemical hydrogen production, Sol. Energ.
501 Mat. Sol. C 141 (2015) 101-107.
502 [36] X. Li, M. Puttaswamy, Z. Wang, C. Kei Tan, A.C. Grimsdale, N.P. Kherani, A.I.Y.
503 Tok, A pressure tuned stop-flow atomic layer deposition process for MoS_2 on high
504 porous nanostructure and fabrication of TiO_2/MoS_2 core/shell inverse opal structure,
505 Appl. Surf. Sci. 422 (2017) 536-543.
506 [37] S.K. Karuturi, C. Cheng, L. Liu, L.T. Su, H.J. Fan, A.I.Y. Tok, Inverse opals
507 coupled with nanowires as photoelectrochemical anode, Nano Energy 1 (2012)
508 322-327.
509 [38] C. Cheng, S.K. Karuturi, L. Liu, J. Liu, H. Li, L.T. Su, A.I.Y. Tok, H.J. Fan,

510 Quantum-dot-sensitized TiO_2 inverse opals for photoelectrochemical hydrogen
511 generation, Small 8 (2012) 37-42.
512 [39] S. Peng, F. Cheng, J. Liang, Z. Tao, J. Chen, Facile solution-controlled growth of
513 $CuInS_2$ thin films on FTO and TiO_2/FTO glass substrates for photovoltaic application,
514 J. Alloys. Compd. 481 (2009) 786-791.
515 [40] C. Tang, Y. Zhang, J. Su, C. Wang, R. Sun, J. Zhang, G. Li, Synthesis and
516 photocatalytic properties of vertically aligned Bi_2S_3 platelets, Solid State Sci. 51
517 (2016) 24-29.
518 [41] W.-Q. Fan, X.-Q. Yu, S.-Y. Song, H.-Y. Bai, C. Zhang, D. Yan, C.-B. Liu, Q.
519 Wang, W.-D. Shi, Fabrication of TiO_2-BiOCl double-layer nanostructure arrays for
520 photoelectrochemical water splitting, CrystEngComm 16 (2014) 820-825.
521 [42] G.V. Govindaraju, G.P. Wheeler, D. Lee, K.-S. Choi, Methods for
522 electrochemical synthesis and photoelectrochemical characterization for
523 photoelectrodes, Chem. Mater. 29 (2016) 355-370.
524 [43] F. Le Formal, N. Tétreault, M. Cornuz, T. Moehl, M. Grätzel, K. Sivula,
525 Passivating surface states on water splitting hematite photoanodes with alumina
526 overlayers, Chem. Sci. 2 (2011) 737-743.
527 [44] L. Wang, W. Wang, Y. Chen, L. Yao, X. Zhao, H. Shi, M. Cao, Y. Liang,
528 Heterogeneous p-n junction CdS/Cu_2O nanorod arrays: synthesis and superior
529 visible-light-driven photoelectrochemical performance for hydrogen evolution, ACS
530 Appl. Mater. Interfaces 10 (2018) 11652-11662.
531 [45] X. Zhou, W. Fu, H. Yang, Y. Mu, J. Ma, L. Tian, B. Zhao, M. Li, Facile
532 fabrication of transparent SnO_2 nanorod array and their photoelectrochemical
533 properties, Mater. Lett. 93 (2013) 95-98.
534 [46] W. Wang, C. Jin, L. Qi, Hierarchical CdS nanorod@SnO_2 nanobowl arrays for

535 efficient and stable photoelectrochemical hydrogen generation, Small (2018)
536 1801352.

537

538